



Universiteit
Leiden
The Netherlands

Neuroimmune guidance cues for vascular health

Zhang, H.

Citation

Zhang, H. (2021, June 1). *Neuroimmune guidance cues for vascular health*. Retrieved from <https://hdl.handle.net/1887/3176518>

Version: Publisher's Version

License: [Licence agreement concerning inclusion of doctoral thesis in the Institutional Repository of the University of Leiden](#)

Downloaded from: <https://hdl.handle.net/1887/3176518>

Note: To cite this publication please use the final published version (if applicable).

Cover Page



Universiteit Leiden



The handle <http://hdl.handle.net/1887/3176518> holds various files of this Leiden University dissertation.

Author: Zhang, H.

Title: Neuroimmune guidance cues for vascular health

Issue date: 2021-06-01

Chapter 4

Endothelial Netrin-4 prevents endothelial cell senescence and promotes endothelial cell survival

Zhang, H., Vreeken, D., Leuning, D. G., Bruikman, C. S., Junaid, A., Stem, W., deBruin, R. G., Sol, W. M. P. J., Rabelink, T. J., van den Berg, B. M., van Zonneveld, A. J. and van Gils, J. M.

International Journal of Biochemistry and Cell Biology, 2021;134.

Abstract

Netrin-4, recognized in neural and vascular development, is highly expressed by mature endothelial cells. The function of this netrin-4 in vascular biology after development has remained unclear. We found that the expression of netrin-4 is highly regulated in endothelial cells and is important for quiescent healthy endothelium. Netrin-4 expression is upregulated in endothelial cells cultured under laminar flow conditions, while endothelial cells stimulated with tumor necrosis factor alpha resulted in decreased netrin-4 expression. Targeted reduction of netrin-4 in endothelial cells resulted in increased expression of vascular cell adhesion molecule 1 and intercellular adhesion molecule 1. Besides, these endothelial cells were more prone to monocyte adhesion and showed impaired barrier function, measured in electric cell-substrate impedance sensing system, as well as in an ‘organ-on-a-chip’ microfluidic system. Importantly, endothelial cells with reduced levels of netrin-4 showed increased expression of the senescence-associated markers cyclin-dependent kinase inhibitor-1 and -2A, an increased cell size and decreased ability to proliferate. Consistent with the gene expression profile, netrin-4 reduction was accompanied with more senescent associated β -galactosidase activity, which could be rescued by adding netrin-4 protein. Finally, using human decellularized kidney extracellular matrix scaffolds, we found that pre-treatment of the scaffolds with netrin-4 increased numbers of endothelial cells adhering to the matrix, showing a pro-survival effect of netrin-4. Taken together, netrin-4 acts as an anti-senescence and anti-inflammation factor in endothelial cell function and our results provide insights as to maintain endothelial homeostasis and supporting vascular health.

Keywords

endothelial cells, netrin-4, senescence, inflammation, barrier function

4.1 Introduction

Endothelium is the interior surface lining of blood vessels. It is involved in physiological regulation of vascular barrier function, hemostasis and controlling of vascular tone. In disease conditions, the endothelium can undergo functional adaptations and plays a role in inflammatory response. Recent studies have identified novel roles of netrin class proteins in these processes[1-4]. Netrin class proteins belong to the broader families of neuronal guidance cues, which were originally identified in the nervous system for their role in directing axon growth, but were later found to have expression and functions in many other tissues [5]. Among netrin family proteins, we and others found netrin-4 (NTN4) to be the most abundantly expressed in endothelial cells[6-8]. NTN4 is a special member of the netrin family in several ways. Firstly, N-terminal domains of NTN4 are homologous to laminin β chain, whereas those of other secreted netrins are homologous to laminin γ chain [5]. Secondly, NTN4 has low binding affinity to the canonical netrin receptors, UNC5B, NEO1 and DCC [9]. Instead, NTN4 has the property to bind to laminin γ chain in a way that could disassemble the laminin network [9, 10]. Through this mechanism, high levels of exogenous NTN4 were shown to disrupt branching of the epithelium in submandibular gland explants and to decrease capillary development in a chick chorioallantoic membrane assay[9, 10]. The involvement of NTN4 in endothelial cell biology is most studied in the context of angiogenesis, though consistency of evidence is still lacking. NTN4 was found to either increase[11, 12] or inhibit[7, 13, 14] endothelial cell migration and tube formation. However, the role of endothelial NTN4 in physiology remains unclear. In this study, we confirmed the high expression of NTN4 in endothelial cells and demonstrated its modulation by inflammation and hemodynamic factors. State-of-art assays were used to further investigate the functional importance of NTN4. We observed a premature cellular senescent phenotype with inflammation and barrier loss upon reduced expression levels of NTN4 by endothelial cells. Furthermore, we found that addition of NTN4 to extracellular matrix favored the survival of endothelial cells.

4.2 Materials and Methods

4.2.1 Access to curated online gene expression datasets

Curated online gene expression datasets from all anatomical types on the microarray platform “Affymetrix Human Genome U133 Plus 2.0 Array” (abbreviation: HG-U133_Plus_2;

accession: GPL570) were obtained using Genevestigator software [15]. Average expression of selected genes from endothelial types of cells and the standard deviation was extracted. A heatmap illustrating the expression values was created with R package ggplot2[16].

4.2.2 Cell culture

Human umbilical vein endothelial cells (HUVECs) were isolated in house from human umbilical cords as described previously [17] and cultured in endothelial growth medium-2 (EGM2, Lonza, CC-3162) supplemented with antibiotics, unless indicated otherwise. Human pulmonary microvascular endothelial cells (MVECs) were a kind gift from Prof. M.J.T.H. Goumans, Leiden University Medical Center, Leiden, the Netherlands. MVECs were culture in microvascular endothelial cell medium-2 (EGM-2-MV, Lonza). Primary human peripheral blood monocytes were isolated as described previously [18] and cultured in RPMI1640 medium (Gibco, 21875034) supplemented with 10% FBS (v/v) and antibiotics. HEK293T cells were purchased from ATCC and cultured in DMEM medium (Gibco, 41965039) supplemented with 10% FBS and antibiotics. All cells were kept at 37 °C with 5% CO₂.

4.2.3 Human tissue

Human transplant grade kidneys that were discarded for surgical reasons were used after research consent was given. Procedures of kidney biopsies and decellularization were adapted from Ott et al.[19] and were previously described by Leuning et al. [20]. In brief, the renal artery was cannulated with a Luer-lock connector (Cole-Parmer, Barendrecht, the Netherlands) and the kidney was perfused with 1% SDS in PBS containing antibiotics, antimycotics, and DNase, under a constant pressure of maximal 75 mm Hg for 5 days. Afterwards the kidneys were perfused with dH₂O with antibiotics, antimycotics, and DNase overnight. Then the kidneys were flushed with 1% (v/v) Triton-X 100 (Sigma) for one day and afterwards flushed with PBS with antibiotics and antimycotics for at least 5 days, all under a constant pressure of max. 75 mm Hg. Kidneys were stored at 4 °C in PBS until further use. Biopsies of $\approx 1 \text{ cm}^3$ were taken and either snap frozen in liquid nitrogen or fixed overnight in 4% formaldehyde (Klinipath, Duiven, the Netherlands), stored in 70% ethanol, embedded in paraffin and cut in 4 μm thick sections. Coronary atherosclerotic plaques were retrieved from the archives of the Department of Pathology, Academic Medical Center, the Netherlands. Materials were obtained after research consent and paraffin embedding.

4.2.4 Quantitative PCR analysis for gene expression

For gene expression analysis, cells were lysed in Trizol (Invitrogen, 15596026). Total RNA was extracted using RNeasy Mini Kit (Qiagen, 74106) according to the manufacturer's manual. Genomic DNA was removed using RNase-Free DNase Set (Qiagen, 79254). First strand complementary DNA was synthesized with equal amount of RNA input using M-MLV Reverse Transcriptase (Promega, M1701) with OligodT primers (Promega, C1101). Quantitative PCR (qPCR) analysis was performed with SYBR Green Master Mix (Applied Biosystems, A25777). List of primers used can be found in **Supplemental table 1**.

4.2.5 Immunohistochemistry or immunofluorescence staining

For immunofluorescence staining of snap frozen human (decellularized) kidney sections, sections were fixed in 4% paraformaldehyde (w/w in PBS) for 10 min at room temperature. The samples were then washed three times with PBS and blocked with Serum-Free Protein Block (Dako, X090930-2) for 30 minutes at room temperature. Primary antibodies were prepared in 1% BSA (w/w in PBS). Incubation of primary antibodies was set at 4 °C overnight. After the incubation, samples were washed three times with PBS again and incubated with Alexa fluorochrome conjugated secondary antibody mix prepared in 1% BSA (w/w in PBS supplemented with Hoechst (1:1000, Invitrogen, 11534886). Sections were then washed three times with PBS and mounted with Prolong Gold (Invitrogen, P36930). For immunohistochemistry staining of human coronary arteries, slides were deparaffinized in 100% xylene and rehydrated in ethanol. Heat-induced epitope retrieval was performed in tris-EDTA buffer (pH 9.0) for 20 minutes at 98°C. Next, nonspecific antigens were blocked with 1% BSA in TBS for 30 minutes, followed by incubation with primary antibody overnight. After washing in TBS slides were incubated with HRP-labeled secondary antibody for one hour and counterstained with Bright DAB substrate kit (BS04-110, Vector laboratories, Burlingame, CA, USA). Slides were covered with glycerol (C0563, Agilent, Glostrup, Denmark) and a glass coverslip. For immunofluorescence staining of HUVECs, cells were washed with Hank's Balanced Salt Solution with calcium and magnesium (HBSS+, Gibco, 14025092) and fixed with 4% formaldehyde (v/v in HBSS+) for 10 minutes at room temperature. The cells were then permeabilized with 0.1% Triton X-100 (w/w in HBSS) for two minutes, washed with HBSS and incubated with 5% BSA (w/w in HBSS+) to reduce non-specific antibody binding. Primary antibody prepared in 0.5% BSA (w/w in HBSS+) was used to incubate the cells overnight at 4 °C: The cells were washed three times. Alexa fluorochrome conjugated

secondary antibody mix was prepared in 0.5% BSA (w/w in HBSS+) supplemented with Hoechst 33528 (1:1000, Invitrogen, 11534886). After incubation with the mix for one hour at room temperature, cells were washed again three times with HBSS+. Fluorescent images were captured using Leica TCS SP5 confocal microscopy system (pinhole 1 airy; imaged 7-8 μm z-distance with step size of about 0.5 μm) and analyzed using ImageJ software. List of antibodies used can be found in **Supplemental table 2**.

4.2.6 Lentiviral vectors, lentiviral particle production and transduction

Four different shRNA constructs targeting human QKI, and four different shRNA constructs targeting human NTN4 were obtained from the Mission Library (Sigma Aldrich), and tested for their efficiency to knockdown QKI or NTN4, respectively. The best shRNAs for targeting QKI or NTN4 were selected to perform all experiments. As a control, a non-targeting shRNA (scramble) was used. Lentiviral particles were produced as described by the Sigma Library protocol using HEK293T cells. Selection of transduced cells was achieved using puromycin (2 $\mu\text{g}/\text{mL}$).

4.2.7 RNA immunoprecipitation

RNA-immunoprecipitation was performed with MVECs using Millipore's validated RIPAb+ QKI-5 kit according to manufacture instructions.

4.2.8 Immunoblot analysis

Endothelial cells were washed with cold PBS and lysed in cold RIPA buffer (Cell signaling, 9806). After centrifugation of the samples at 14000rpm for 10 minutes at 4 °C, protein concentration in the supernatant was measured using the Pierce BCA Protein Assay Kit (Thermo Scientific, 23255). Equal amounts of protein sample were denatured using DTT and heating at 95 °C for 10 minutes followed by size separation on a 10% Mini-PROTEAN gel (Biorad, 4561033). Proteins were transferred to PVDF membranes (Biorad, 1704156) using the Trans-Blot Turbo system (Biorad), after which membranes were blocked in either TBST-5% BSA (Sigma, A2058) for phosphorylated proteins or TBST-5% milk. Overnight incubation was performed with primary antibodies. Incubation with HRP-conjugated secondary antibodies (1:5000, Dako) and Western lightning ECL (PerkinElmer, NEL103001EA) or SuperSignal Western Blot Enhancer (ThermoFisher, 46640) enabled us to visualize protein bands with the ChemiDoc Touch Imaging System (Biorad). Expression was quantified using ImageLab software (Biorad) and ImageJ software (<http://rsbweb.nih.gov/ij/>). List of

antibodies used can be found in **Supplemental table 2**.

4.2.9 Proliferation assay

MTT (3-(4,5-dimethylthiazol-2-yl)-2,5-diphenyltetrazolium bromide), a yellow tetrazole, can be reduced to purple formazan by living cells. Thus, the number of viable cells can be quantified in colorimetric manner. HUVECs were seeded in 24-well plates in subconfluent density to allow space to proliferate (10,000 cells per well). At day one, three and five after seeding, 3-(4,5-dimethylthiazol-2-yl)-2,5-diphenyltetrazolium bromide (MTT) solution (0.5 $\mu\text{g}/\text{mL}$ in PBS) was added to designated wells after a wash with PBS. The cells were incubated for 30 minutes at 37 °C. After the incubation, MTT solution was removed and 150 μL acidified isopropanol (0.04 M hydrochloride acid in isopropanol) solution was added to lyse the cells. The lysate was transferred to a 96-well plate. Colorimetric reading was done at 562 nm.

4.2.10 Senescence associated β -galactosidase staining

Senescence associated β -galactosidase staining was done using Senescence Cell Histochemical Staining Kit (Sigma, CS0030) according to the manufacturer's protocol. Briefly, HUVECs were seeded in subconfluent density (10,000 per cm^2) in μs slides (IBIDI, 80826). After overnight culture, cells were washed twice with PBS and fixed with 1x Fixation Buffer for six minutes. After fixation, cells were washed three times with PBS. The staining mixture (200 μL) was added to each well and allowed to incubate overnight at 37 °C. After staining, the number of positively stained cells (blue) and total cells were counted per field of view. Percentage of positively stained cells was calculated for each condition.

4.2.11 Adhesion assay of primary monocytes to endothelial cell monolayer

HUVECs were seeded at confluent density (40,000 per cm^2) one day before the experiment in 96-well plates. Peripheral blood was obtained after informed consent (Ethical Approval Number BTL 10.090) and peripheral mononuclear cells were isolated by density gradient separation using Ficoll. CD14 Microbeads (Miltenyi Biotec, 130-050-201) and LS columns (Miltenyi Biotec, 130-042-401) were used for magnetic separation of CD14 positive monocytes. Freshly isolated monocytes were labelled with 5 $\mu\text{g}/\text{mL}$ Calcein AM (Molecular Probes Life Technologies, C3100MP) and incubated on top of a monolayer of HUVECs for 30 minutes at 37 °C. Non-adhering cells were washed away by multiple washing steps with PBS, after which images were made. Cells were then lysed in Triton-X 1% for 10 minutes.

Fluorescence was measured at λ_{ex} 485 nm and λ_{em} 514 nm.

4.2.12 Electric cell-substrate impedance sensing

Electric Cell-substrate Impedance Sensing (ECIS) assays were done using the ECIS Ztheta device (Applied BioPhysics) with standard 8-well arrays (Applied BioPhysics, 8W10E). The 8-well arrays had gold electrodes fixed onto the bottom of the wells, enabling real time measurement of impedance, which represents endothelial barrier function. Prior to the experiment, electrodes were pretreated using 10 mM L-cysteine for 10 minutes. The wells were washed twice using water and coated with 0.5% gelatin (w/w in water) for 10 minutes. Gelatin solution was then replaced by 400 μ L EGM2 medium and cell free baseline measurements were taken for approximately 30 minutes. Meanwhile, HUVECs were trypsinized and resuspended at a concentration of 1×10^6 per 200 μ L. The measurements were paused, 1×10^6 HUVECs were added to each well in the volume of 200 μ L. The measurements were then resumed for at least 24 hours. Measurements were taken at multiple frequencies every five minutes. Readings at 4000 Hz were used for data analysis and illustration, because at this frequency the impedance measurement is mainly contributed by cell-cell junction resistance.

4.2.13 Permeability of 3D endothelial culture

HUVECs with or without NTN4 knockdown were seeded in gelatin coated microvascular channels of custom-made gradient design OrganoPlate® (Mimetas) with 4 mg/mL type 1 collagen (Trevigen) in the extracellular matrix channel. After allowing the cells to adhere for one hour, culture medium was replaced by a mix of Endothelial Cell Growth Medium MV2 (PromoCell) and Pericyte Growth Medium (Angio-Proteomie) in a ratio of 1:1. The device was placed on a rocker platform with 7° angle of motion and eight minutes timed operation to allow continuous flow of medium in the microvessels. After 24 hours, the medium was refreshed and the HUVECs were cultured for 3-4 more days. To measure vessel permeability, the culture medium in the microvascular channels was replaced with culture medium containing 125 μ g/mL Albumin-Alexa 555 (Life Technologies). Following this, the OrganoPlate® was placed in the environmental chamber (37 °C; 5% CO₂) of a fluorescent microscope system (Nikon Eclipse Ti) and time-lapse images were captured. The permeability coefficient was calculated by determining the fluorescent intensities in the microvascular channel and in the extracellular matrix channel. The fluorescent intensity of the extracellular matrix channel was normalized with the fluorescent intensities in the

microvascular channel of each measured time point. This showed the change in intensity ratio inside the gel channel as a function of time. The scatter plot was fitted with a linear trend line to determine the slope. Finally, using Fick's First Law, the apparent permeability was determined as:

$$P_{app}(\cdot 10^{-6} \text{ cm/s}) = \frac{d\left(\frac{I_g}{I_p}\right)}{dt} \cdot \frac{A_g}{l_w} \quad (4.1)$$

where I_p is the intensity in the microvascular channel, I_g is the intensity in the ECM channel, $A_g(480 \cdot 10^{-6} \text{ cm}^2)$ is the area of the ECM channel and l_w is the length of the vessel wall that separates between ECM and microvascular region. All data analysis was done with ImageJ (<http://rsbweb.nih.gov/ij/>, NIH, United States) and Matlab (MathWorks).

4.2.14 Decellularized human kidneys

For pretreatment of NTN4 on decellularized kidney sections, the snap frozen sections of decellularized kidneys were prepared on coverslips, placed in 24 wells plate and incubated with recombinant human NTN4 (1 $\mu\text{g/mL}$ in 200 μL PBS, R&D systems, 1254-N4-025) overnight at 4 $^{\circ}\text{C}$. Incubation using only PBS served as a control. The next day, NTN4 solution was removed and, when indicated, 5e4 HUVECs were seeded into the wells to allow the interaction between HUVECs and the kidney extracellular matrix. The cells were cultured for 24 hours at 37 $^{\circ}\text{C}$, before being fixed with 4% paraformaldehyde (w/w in PBS) for one hour at room temperature. Immunofluorescent staining of laminin, NTN4 and CD31 was performed as described in the immunofluorescent staining section.

4.2.15 Statistical analyses

The difference between two group means was analyzed by Student's t-test. Comparison of three group means was analyzed by one-way ANOVA with Dunnett's post hoc analysis for the paired comparison to the control group. Mix effects of two conditions were analyzed by two-way ANOVA with the interaction term. P values of less than 0.05 were considered significant for all types of statistical analyses.

4.3 Results

4.3.1 NTN4 is the highest expressed Netrin in endothelial cells

We set off by studying the expression of NTN4 in various kinds of endothelial cells using available transcriptomics data on the GPL570 platform, a commonly used human transcriptome microarray platform. The average expression values of netrin family genes are

presented in a heatmap, and expression of cadherin 5 (CDH5, vascular endothelial cadherin) and cadherin 1 (CDH1, epithelial cadherin) were taken along as references of genes with high or low expression (**Figure 1A**). NTN4 is the highest expressed netrin family gene in all endothelial cell types, except for bone marrow endothelial progenitor cells. In some endothelial cell types, NTN4 expression is comparable to that of CDH5, which encodes one of the main components of endothelial adherens junctions. We also compared the NTN4 expression of endothelial cell types to that of other cell types by ranking all cell types by NTN4 expression. The ranking resulted in seven endothelial cells types and the capillary-rich structure of glomerulus in the top-10 list, confirming higher expression of NTN4 in endothelial cells relative to other cell types (**Figure 1B**). The high expression of NTN4 in HUVECs was confirmed by qPCR (**Figure 2A**). In accordance to the gene expression data, protein expression of NTN4 was observed in the endothelium of human coronary artery (**Figure 2B**), and in the glomeruli and peritubular micro-vessels of human kidney (**Figure 2C**). Consistent with the fact that NTN4 is secreted to endothelial basement membrane, staining of NTN4 co-localized with laminin signal at areas of vascular structures (**Figure 2C**).

4.3.2 Inflammation reduces and laminar shear stress induces NTN4 expression in endothelial cells

Given the high expression of NTN4 in endothelial cells, we next assessed if inflammatory and hemodynamic conditions could affect the expression of NTN4. Stimulation of HUVECs with the inflammatory cytokines tumor necrosis factor (TNF α) and interleukin 1 β (IL1 β) decreased the expression of NTN4 (**Figure 3A**), while culturing the cells under prolonged laminar flow conditions upregulated expression of NTN4 (**Figure 3B, C, Supplementary Figure 1**). Using confocal microscopy, NTN4 staining was found to be apparent in vesicles, consistent with NTN4 being a secreted protein (**Figure 3C and Supplementary Figure 1**). In addition, we observed no clear NTN4 staining at the extracellular basement membrane itself (**Supplementary Figure 1**). As the RNA-binding protein Quaking (QKI), discovered as post-transcriptional regulator and important for the development of central nervous system[21, 22], is also regulated in the same manner by flow conditions [17] (**Figure 3D**), we investigated the role of QKI in regulating NTN4 expression. Knockdown of QKI (**Supplementary Figure 2A**) suppressed the expression of NTN4 in endothelial cells (**Figure 3E**). We next sought to determine whether QKI can directly bind to mRNA

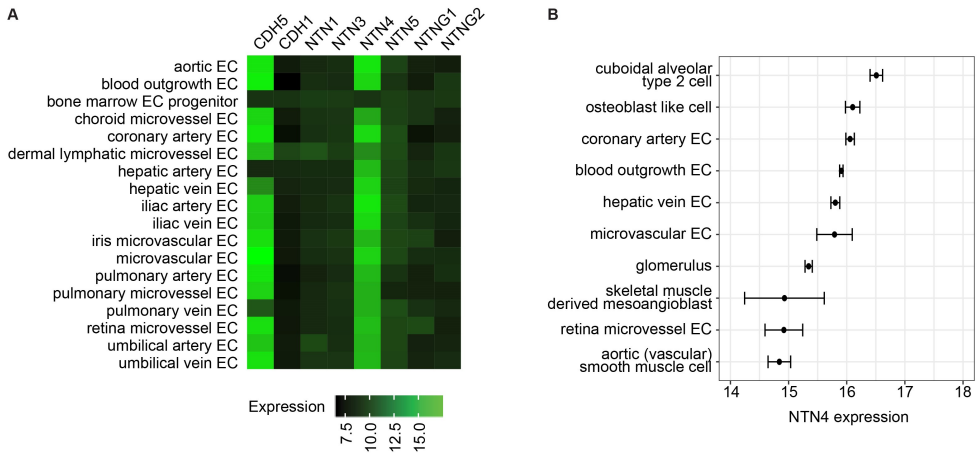


Figure 1. High expression of NTN4 in various types of endothelial cells

(A) Heatmap of netrin family expression in all types of human endothelial cells profiled on Affymetrix Human Genome U133 Plus 2.0 Array platform (GEO accession: GPL570). Numbers indicate normalized microarray signals on log₂ scale. Black color: lower expression and green color: higher expression. Expression signals of CDH5 and CDH1 were included as references. (B) NTN4 expression in 10 human cell types with highest NTN4 expression. Data is presented as Mean ± SEM; n ≥ 3.

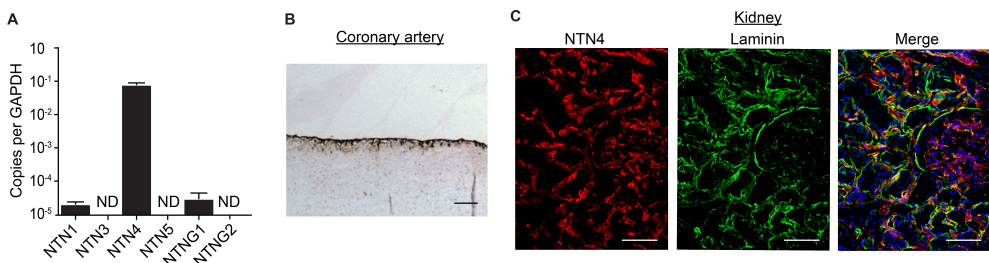


Figure 2. Confirmation of NTN4 expression in endothelial cells

(A) Quantification of expression of the netrin family with qPCR in HUVECs. Results are presented as copy numbers per GAPDH, Mean ± SEM, n = 5. (B) Immunohistochemistry of NTN4 (brown) in human coronary artery. Scale bar = 50 μm. (C) Immunofluorescent staining of NTN4 (red), laminin (green) and DNA (blue) in human kidney sections. Scale bars: 100 μm

of NTN4 using an RNA-immunoprecipitation experiment. Indeed, mRNA of NTN4 was highly enriched in the QKI-antibody precipitated RNA fraction (**Figure 3F, G**), indicating binding of QKI to NTN4 mRNA.

4.3.3 Reducing NTN4 promotes an inflammatory phenotype in endothelial cells

In order to study the functional importance of NTN4 for endothelial cells, NTN4 expression in endothelial cells was silenced using lentiviral shRNA vectors targeting NTN4 mRNA. A non-NTN4 targeting scrambled shRNA was used as a control. Repression of NTN4 was validated using qPCR and immunofluorescence staining (**Supplementary Figure 2B, C**). Staining of endothelial cells with reduced levels of NTN4 compared to endothelial cells transduced with scrambled shRNA showed less aligned adherens junctions, made visible by Cadherin 5 staining. Using antibodies binding to an epitope of the integrin $\beta 1$ that is exposed constitutively or only exposed upon activation, respectively [23, 24], we showed that endothelial cells with reduced levels of NTN4 have more total and activated integrin $\beta 1$ (**Figure 4A, B, Supplementary Figure 3**). As increased integrin activity levels can be induced by inhibition of protein kinase B (PKB, also known as Akt) [25, 26], we investigated Akt phosphorylation levels using western blot. Reducing NTN4 in endothelial cells resulted in less P-Akt (**Figure 4C**).

In addition, we investigated whether loss of NTN4 induces vascular leakage, since the morphological change with less aligned adherens junctions strongly indicates the possibility of reduced endothelial barrier function. In both electric cell-substrate impedance sensing (ECIS) system [27] and the more physiological 3D-endothelial tube in a microfluidics platform [28], we found that targeted reduction of NTN4 in endothelial cells resulted in impaired barrier function (**Figure 5A, B**). Since reduction in endothelial barrier function is often caused by an inflammatory phenotype, we examined whether the NTN4 knockdown endothelial cells are more inflammatory-like. Endothelial cells with NTN4 KD indeed showed more adhesion of primary monocytes (**Figure 5C**) and exhibited elevated expression of ICAM1 and VCAM1 both at mRNA and protein levels (**Figure 5D, E**).

4.3.4 Reducing NTN4 induces endothelial cell senescence

Next to the inflammatory phenotype, we observed enlarged cell bodies at the same seeding density (**Figure 6A**) and reduced capacity to proliferate (**Figure 6B**) in endothelial cells with reduced expression of NTN4. These observations prompted us to assess cell senes-

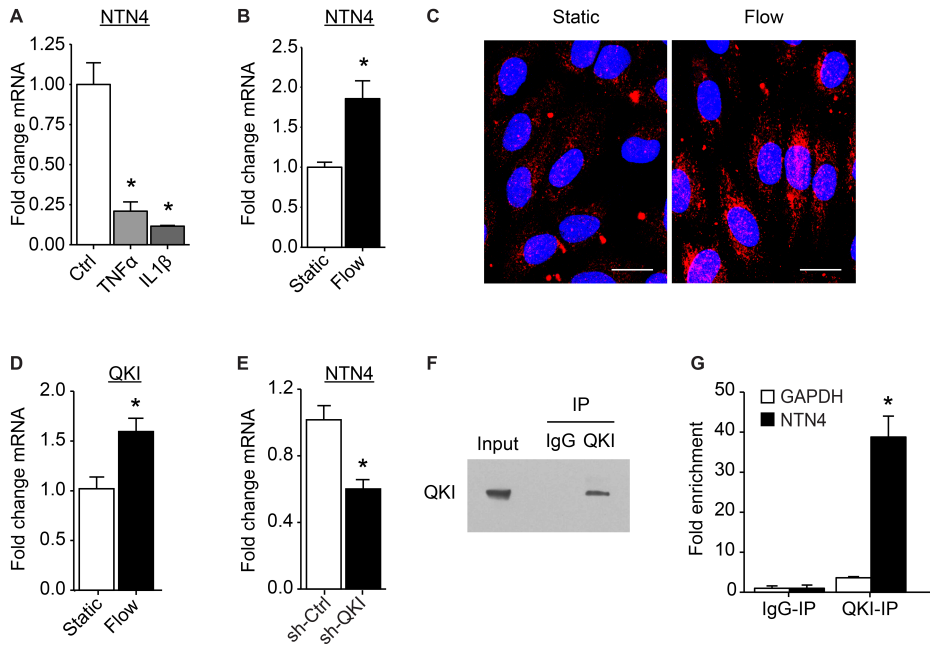


Figure 3. Regulation of NTN4 expression level in HUVECs

(A-B) qPCR analysis of NTN4 mRNA isolated from (A) HUVECs stimulated with the inflammatory factors, TNF α (10 ng/mL) or IL1 β (20 ng/mL) for 24 hours, or (B) HUVECs cultured under static conditions or laminar flow (10 dynes/cm²) conditions for seven days. Results are expressed as fold change of untreated cells (A) or static cultured cells (B), set to 1, Mean \pm SEM, n = 3; * p < 0.05. (C) Immunofluorescence staining of NTN4 (red) and DNA (blue) in HUVECs cultured under static conditions or laminar flow (10 dynes/cm²). Maximum intensity z -projection images from a series of confocal images. Scale bars = 20 μ m (D) qPCR analysis of QKI mRNA isolated from HUVECs cultured under static or laminar flow conditions. Results are presented relative to static cultured cells. Mean \pm SEM of n = 4. * p < 0.05. (E) qPCR analysis of NTN4 mRNA isolated from HUVECs transduced with anti-Qki shRNA (shQKI) or control shRNA (shCtrl). Results are presented relative to shCtrl. Mean \pm SEM of n = 5. * p < 0.05. (F, G) RNA-immunoprecipitation in HUVEC using an IgG control or QKI-5 antibody. (F) Immunoblot of QKI confirming immunoprecipitation of QKI protein from endothelial cell lysates. (G) NTN4 and GAPDH mRNA abundance in the immune-precipitated fraction was determined by qPCR. Results are presented relative to IgG immunoprecipitation. Mean \pm SEM of n = 4. * p < 0.05.

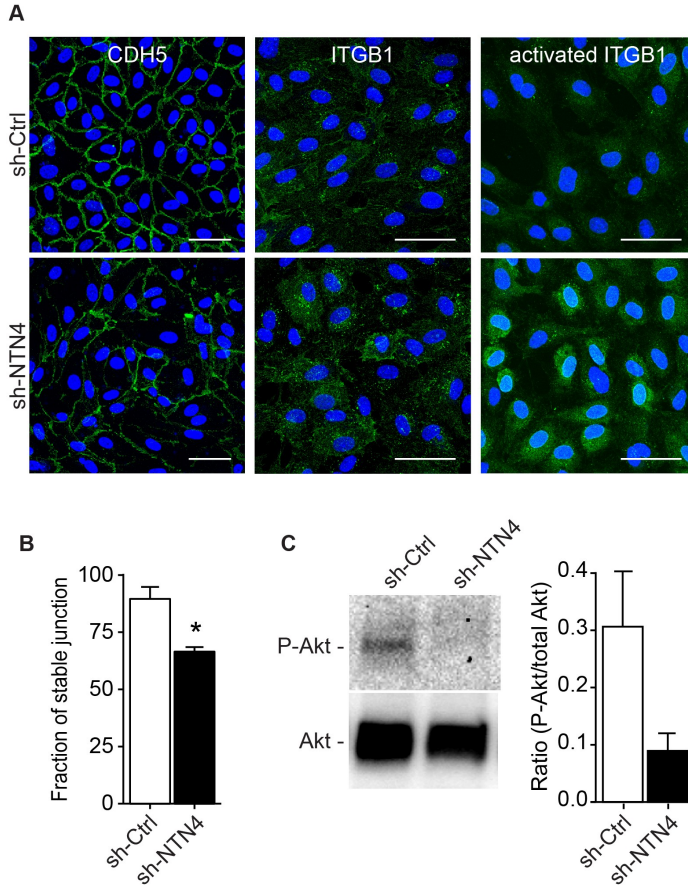


Figure 4. Reduction of NTN4 expression in endothelial cells reduces CDH5 junction localization and increases integrin β 1 activity

(A) Immunofluorescence staining of CDH5, integrin β 1 or activated integrin β 1 (green) and DNA (blue) in HUVECs transduced with anti-NTN4 shRNA (sh-NTN4) or scrambled shRNA (sh-Ctrl). Representative images of $n = 2-3$. Maximum intensity z -projection images from series of confocal images. Scale bar = 50 μ m. (B) Quantification of fraction of stable adherens junctions. Mean \pm SEM of $n = 3$; * $p < 0.05$. (C) Immunoblots and quantification of phospho- and total Akt in sh-Ctrl and sh-NTN4 treated cells. Levels are expressed as ratio P-Akt/total Akt, Mean \pm SEM of $n = 3$.

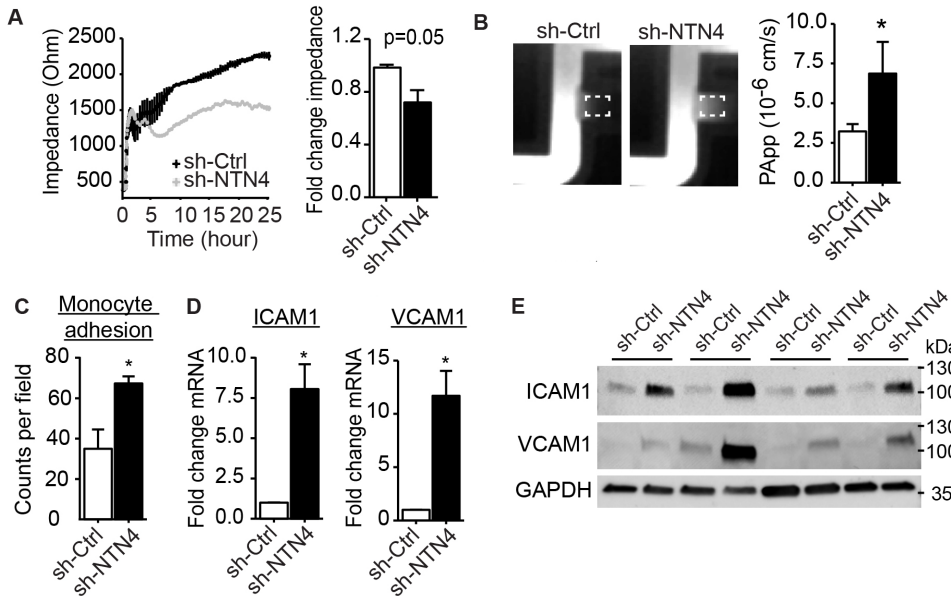


Figure 5. Reduction of NTN4 expression in endothelial cells diminishes endothelial barrier function and promotes an inflammatory phenotype

(A) Left graph shows transendothelial electrical resistance of scrambled shRNA (sh-Ctrl) or anti-NTN4 shRNA (sh-NTN4) transduced HUVECs seeded on electric cell-substrate impedance sensing (ECIS) electrodes (Mean \pm SD of technical triplicates, representative of three independent experiments). Right graph shows the relative trans-endothelial electrical resistance of sh-Ctrl or sh-NTN4 HUVEC stable monolayer, sh-Ctrl set to 1. Mean \pm SEM of $n = 3$. (B) HUVECs transduced with sh-Ctrl or sh-NTN4 were seeded in the vertical channel of a microfluidic device with collagen in the horizontal channel. At the start of the measurement, fluorescently labeled albumin was infused in the vessel lumen and after 10 minutes albumin leakage outside the vessel channel was visualized and quantified. Dotted box indicates the region used in quantification. Bar graph shows the permeability coefficient presented as Mean \pm SEM of $n = 3$; * $p < 0.05$. (C) Quantification of adhesion of primary human monocytes to sh-Ctrl or sh-NTN4 transduced HUVECs. Mean \pm SEM of $n = 3$; * $p < 0.05$ (D) ICAM1 and VCAM1 mRNA expression in sh-Ctrl or sh-NTN4 transduced HUVECs. Results are presented relative to sh-Ctrl. Mean \pm SEM of $n = 3$; * $p < 0.05$. (E) Immunoblots of ICAM1, VCAM1 and GAPDH (housekeeping) in sh-Ctrl and sh-NTN4 treated cells. $n=4$.

cence by investigating expression levels of senescence-associated transcription factors. Up-regulation of senescence-associated transcription factors, CDKN1A and CDKN2A (encoding p21^{Waf1/Cip1} and p16^{Ink4a}, respectively), but not CDKN1B (encoding p27^{Kip1}), was observed in endothelial cells with NTN4 knockdown (**Figure 6C**). For CDKN1A, the most abundantly expressed of these three genes, we performed immunofluorescence staining to look into protein expression, and observed also at protein level increased expression of the senescence marker CDKN1A upon NTN4 knockdown (**Figure 6D**). Furthermore, senescence-associated β -galactosidase (SA- β -gal) staining revealed a higher percentage of positively stained cells in NTN4 sh-RNA treated endothelial cells compared to scrambled sh-RNA (**Figure 6E**). To confirm the hypothesis that loss of NTN4 induced the endothelial senescence, we performed rescue experiment with human NTN4 protein. Indeed, NTN4 knockdown endothelial cells cultured on human NTN4 coating no longer showed increased β -galactosidase staining compared to control cells (**Figure 6E**).

4.3.5 NTN4 promotes endothelial cell survival

As introduced previously, NTN4 can interact with laminin gamma chain in the basement membrane [9, 10]. To study the consequence for endothelial cells of NTN4 interacting with extracellular matrix, we utilized sections of decellularized human kidney. Immunostaining confirmed NTN4 presence on the extracellular matrix, which could be increased by addition of NTN4 protein (**Figure 7A**). Next, we added endothelial cells to the kidney scaffold with or without extra loading of NTN4. We observed that more endothelial cells adhered to the kidney scaffolds loaded with NTN4, as quantified by CD31 staining and nucleus counting (**Figure 7B and 7C**).

4.4 Discussion

Shear stress, or the in vivo hemodynamic environment, is one of the most profound regulators of endothelial cell biology. Low shear stress or disturbed flow explains the increased vulnerability of certain vascular regions (bifurcations or inner wall of aorta) to pathophysiological changes, such as endothelial senescence, vascular wall inflammation and atherosclerosis [29]. In the current study, we found that the expression of NTN4 could be induced by prolonged laminar shear stress. Making use of NTN4 knockdown endothelial cells, we showed that a reduction of NTN4 resulted in a more inflammatory phenotype with impaired barrier function as well as increased monocyte adhesion due to increased expression of ad-

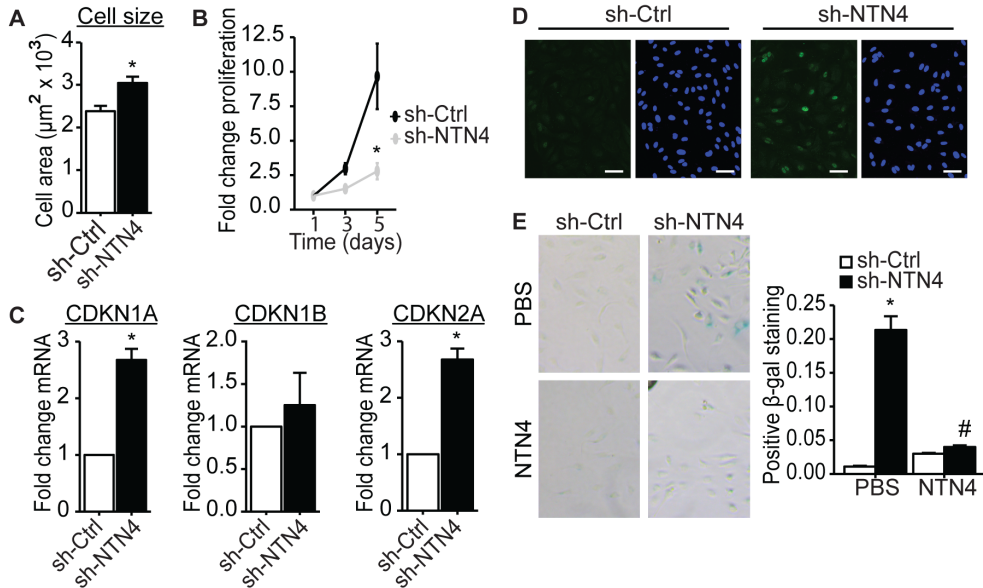


Figure 6. Loss of NTN4 results in endothelial cell senescence

(A) Cell surface area of scramble shRNA treated endothelial cells (sh-Ctrl) or endothelial cells treated with shRNA against NTN4 (sh-NTN4) cultured into confluent monolayer. Mean \pm SEM of $n = 3$; * $p < 0.05$. (B) Proliferation of sh-Ctrl and sh-NTN4 endothelial cells. Results are expressed as fold change to day 0, sh-Ctrl. Mean \pm SEM of $n = 3$; * $p < 0.05$. (C) CDKN1A, CDKN1B and CDKN2A mRNA expression in sh-Ctrl or sh-NTN4 endothelial cells. Results are presented relative to sh-Ctrl set to 1. Mean \pm SEM of $n = 3$; * $p < 0.05$. (D) Immunofluorescence staining of CDKN1A (green) and DNA (blue) in HUVECs transduced with anti-NTN4 shRNA (sh-NTN4) or scrambled shRNA (sh-Ctrl). Representative images of $n = 2$. Maximum intensity z -projection images from series of confocal images. Scale bar = 50 μm . (E) Representative images of SA- β -gal staining of sh-Ctrl or sh-NTN4 cells cultured in wells pre-treated with PBS or NTN4. Bar graph shows the fraction of positively stained cells. Mean \pm SEM of $n = 3$; * $p < 0.05$ for effect of shNTN4, # $p < 0.05$ for interaction effect of shNTN4 and NTN4 coating.

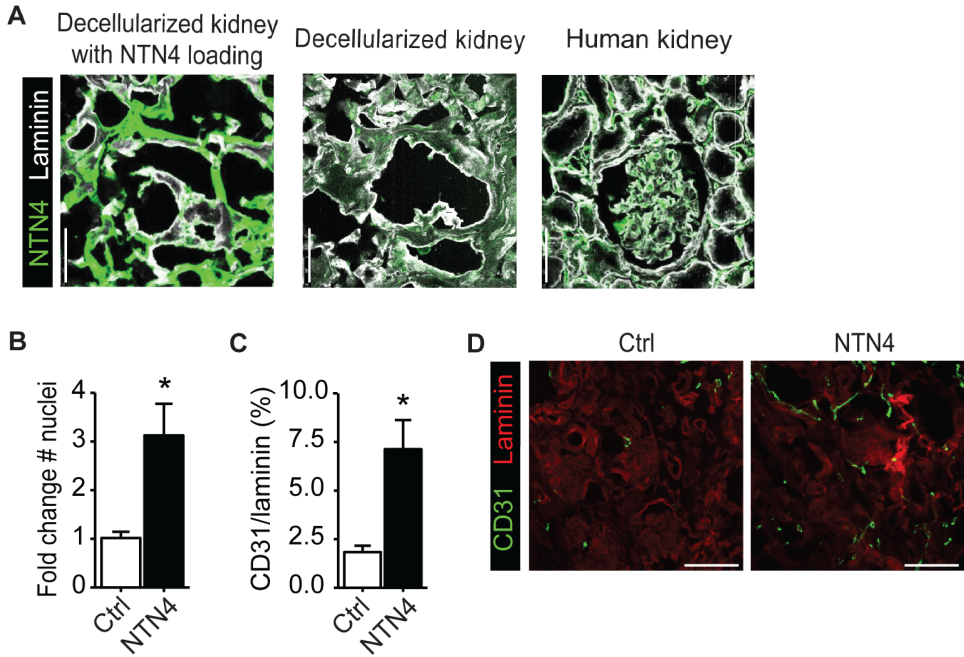


Figure 7. NTN4 on extracellular matrix supports endothelial survival

(A) Immunofluorescence staining of NTN4 (green) and laminin (white) of human kidney and decellularized kidney with and without preincubation of NTN4 protein. Representative images of $n = 3$. Scale bar = 100 μm . (B-C) Number of nuclei (B) or CD31+ area of human decellularized kidneys without (Ctrl) and with preincubation of NTN4 protein (NTN4) on which endothelial cells were added and cultured. Results are expressed as (B) fold change to Ctrl or (C) CD31+/laminin ratio. Mean \pm SEM of $n = 3$; * $p < 0.05$. (D) Immunofluorescence staining of CD31 (green) and laminin (red) of human decellularized kidney with and without preincubation of NTN4 on which endothelial cells were added and cultured. Representative images of $n = 3$. Scale bar = 100 μm .

hesion molecules. Loss of NTN4 also led to a senescent endothelial phenotype, which can explain the inflammatory nature of these cells. Using decellularized human kidneys, we were able to illustrate the effect of NTN4 addition in promoting endothelial adhesion and survival to extracellular matrix. Collectively, these results indicate an important role for NTN4 in maintaining endothelial cell function. Cellular senescence can be induced by two mechanisms, namely replicative senescence and stress-induced senescence. Via these mechanisms, senescence of endothelial cells was shown to occur under circumstances of repetitive injuries (due to atherosclerosis or artificial injuries) or oxidative stress (reviewed in [30]). Replicative senescence results from shortening of telomeres during division of primary cells [31], while stress-induced senescence can be caused by reasons including DNA damage [32] and oxidative stress [33]. We saw senescent phenotypes of endothelial cells upon knockdown of NTN4 expression, which fits in the theoretical framework of stress-induced cellular senescence, since the replicative potential of the HUVECs was not exhausted. Work done by Li et al. showed that NTN4 was implicated in protection of glioblastoma cell line U251MG from senescence in an ITGB4-dependent manner [34]. Further investigations are needed to clarify the dependency of protective effect of NTN4 from senescence on integrin activity in endothelial cells. The presence of NTN4 has been shown to increase activity of Akt and ERK1/2[11, 35]. Increased levels of Akt phosphorylation result in decreased integrin activity[25, 26] and are associated with increased survival of endothelial cells [36]. In line with this, our NTN4 knockdown cells showed decreased Akt phosphorylation, increased integrin activity and decreased endothelial survival. In addition, integrin activity and binding to extracellular matrix also modulate endothelial cell cytoskeletal contractility and cell shape, thereby also affecting endothelial barrier function[37, 38]. ITGB1 gene inactivation impairs proper localization of VE-cadherin and thereby endothelial junction integrity [39]. In contrast, addition of NTN4 has been shown to be able to bind to and activate endothelial integrin alpha 6 beta 1[40]. As NTN4 is structurally homologous to laminin β chain and has been known as a guidance cue in extracellular matrix, it is able to regulate the structure of the laminin network in cellular basement membrane[9, 10]. We suggest that the local concentration of NTN4 is of much relevance. NTN4 has been shown to disassemble laminin networks and to disrupt endothelial basement membrane functions when given exogenously [9]. Here, we demonstrate for the first time that reduction of NTN4 expression from its normal level induces an inflammatory and senescent phenotype. In addition, reintroducing NTN4 can rescue the senescent phenotype and increase adhesion of endothelial cells to the

extracellular matrix. This suggests that modification of the matrix by NTN4 adapts the extracellular matrix properties in a more beneficial way, giving an essential role for NTN4 to regulate endothelial extracellular matrix properties under physiological condition. The relevance of such a modification in vivo is yet to be revealed. Together we identified NTN4 as an anti-senescence and anti-inflammatory protein. NTN4 is important in prevention of endothelial cells from pathophysiological consequences, such as decreased regeneration capacity and endothelial dysfunction.

Acknowledgements

We thank Mehdi Maanaoui and Zsofia Nagy for their technical support. This research was funded by Dutch Heart Foundation, grant number 2013T127, 2018T095, and RECONNECT CVON, European Research Area Network on Cardiovascular Diseases, grant number 038 MISsCVD, and ZonMW MKMD, grant number 114022501.

Conflicts of Interest

The authors declare no conflict of interest.

References

1. Zhang, H., D. Vreeken, C.S. Bruikman, A.J. van Zonneveld, and J.M. van Gils, *Understanding netrins and semaphorins in mature endothelial cell biology. Pharmacol Res*, 2018. 137: p. 1-10.
2. Castets, M., M.M. Coissieux, C. Delloye-Bourgeois, L. Bernard, J.G. Delcros, A. Bernet, V. Laudet, and P. Mehlen, *Inhibition of endothelial cell apoptosis by netrin-1 during angiogenesis. Dev Cell*, 2009. 16(4): p. 614-20.
3. Toque, H.A., A. Fernandez-Flores, R. Mohamed, R.B. Caldwell, G. Ramesh, and R.W. Caldwell, *Netrin-1 is a novel regulator of vascular endothelial function in diabetes. PLoS One*, 2017. 12(10): p. e0186734.
4. van Gils, J.M., B. Ramkhelawon, L. Fernandes, M.C. Stewart, L. Guo, T. Seibert, G.B. Menezes, D.C. Cara, C. Chow, T.B. Kinane, E.A. Fisher, M. Balcells, J. Alvarez-Leite, A. Lacy-Hulbert, and K.J. Moore, *Endothelial expression of guidance cues in vessel wall homeostasis dysregulation under proatherosclerotic conditions. Arterioscler Thromb Vasc Biol*, 2013. 33(5): p. 911-9.
5. Lai Wing Sun, K., J.P. Correia, and T.E. Kennedy, *Netrins: versatile extracellular*

- cues with diverse functions. Development, 2011. 138(11): p. 2153-69.*
6. Podjaski, C., J.I. Alvarez, L. Bourbonniere, S. Larouche, S. Terouz, J.M. Bin, M.A. Lecuyer, O. Saint-Laurent, C. Larochelle, P.J. Darlington, N. Arbour, J.P. Antel, T.E. Kennedy, and A. Prat, *Netrin 1 regulates blood-brain barrier function and neuroinflammation. Brain, 2015. 138(Pt 6): p. 1598-612.*
 7. Nacht, M., T.B. St Martin, A. Byrne, K.W. Klinger, B.A. Teicher, S.L. Madden, and Y. Jiang, *Netrin-4 regulates angiogenic responses and tumor cell growth. Exp Cell Res, 2009. 315(5): p. 784-94.*
 8. Han, Y., Y. Shao, T. Liu, Y.L. Qu, W. Li, and Z. Liu, *Therapeutic effects of topical netrin-4 inhibits corneal neovascularization in alkali-burn rats. PLoS One, 2015. 10(4): p. e0122951.*
 9. Reuten, R., T.R. Patel, M. McDougall, N. Rama, D. Nikodemus, B. Gibert, J.G. Delcros, C. Prein, M. Meier, S. Metzger, Z. Zhou, J. Kaltenberg, K.K. McKee, T. Bald, T. Tuting, P. Zigrino, V. Djonov, W. Bloch, H. Clausen-Schaumann, E. Poschl, P.D. Yurchenco, M. Ehrbar, P. Mehlen, J. Stetefeld, and M. Koch, *Structural decoding of netrin-4 reveals a regulatory function towards mature basement membranes. Nat Commun, 2016. 7: p. 13515.*
 10. Schneiders, F.I., B. Maertens, K. Bose, Y. Li, W.J. Brunken, M. Paulsson, N. Smyth, and M. Koch, *Binding of netrin-4 to laminin short arms regulates basement membrane assembly. J Biol Chem, 2007. 282(33): p. 23750-8.*
 11. Lambert, E., M.M. Coissieux, V. Laudet, and P. Mehlen, *Netrin-4 acts as a pro-angiogenic factor during zebrafish development. J Biol Chem, 2012. 287(6): p. 3987-99.*
 12. Larrieu-Lahargue, F., A.L. Welm, K.R. Thomas, and D.Y. Li, *Netrin-4 induces lymphangiogenesis in vivo. Blood, 2010. 115(26): p. 5418-26.*
 13. Dakouane-Giudicelli, M., S. Brouillet, W. Traboulsi, A. Torre, G. Vallat, S. Si Nacer, M. Vallee, J.J. Feige, N. Alfaidy, and P. de Mazancourt, *Inhibition of human placental endothelial cell proliferation and angiogenesis by netrin-4. Placenta, 2015. 36(11): p. 1260-5.*
 14. Lejmi, E., L. Leconte, S. Pedron-Mazoyer, S. Ropert, W. Raoul, S. Lavalette, I. Bouras, J.G. Feron, M. Maitre-Boube, F. Assayag, C. Feumi, M. Alemany, T.X. Jie,

- T. Merkulova, M.F. Poupon, M.M. Ruchoux, G. Tobelem, F. Sennlaub, and J. Plouet, *Netrin-4 inhibits angiogenesis via binding to neogenin and recruitment of Unc5B*. *Proc Natl Acad Sci U S A*, 2008. 105(34): p. 12491-6.
15. Hruz, T., O. Laule, G. Szabo, F. Wessendorp, S. Bleuler, L. Oertle, P. Widmayer, W. Gruissem, and P. Zimmermann, *Genevestigator v3: a reference expression database for the meta-analysis of transcriptomes*. *Adv Bioinformatics*, 2008. 2008: p. 420747.
16. Wickham, H., *ggplot2: Elegant Graphics for Data Analysis*. Springer-Verlag New York, 2016.
17. de Bruin, R.G., E.P. van der Veer, J. Prins, D.H. Lee, M.J. Dane, H. Zhang, M.K. Roeten, R. Bijkerk, H.C. de Boer, T.J. Rabelink, A.J. van Zonneveld, and J.M. van Gils, *The RNA-binding protein quaking maintains endothelial barrier function and affects VE-cadherin and beta-catenin protein expression*. *Sci Rep*, 2016. 6: p. 21643.
18. de Bruin, R.G., L. Shiue, J. Prins, H.C. de Boer, A. Singh, W.S. Fagg, J.M. van Gils, J.M. Duijs, S. Katzman, A.O. Kraaijeveld, S. Bohringer, W.Y. Leung, S.M. Kielbasa, J.P. Donahue, P.H. van der Zande, R. Sijbom, C.M. van Alem, I. Bot, C. van Kooten, J.W. Jukema, H. Van Esch, T.J. Rabelink, H. Kazan, E.A. Biessen, M. Ares, Jr., A.J. van Zonneveld, and E.P. van der Veer, *Quaking promotes monocyte differentiation into pro-atherogenic macrophages by controlling pre-mRNA splicing and gene expression*. *Nat Commun*, 2016. 7: p. 10846.
19. Guyette, J.P., S.E. Gilpin, J.M. Charest, L.F. Tapias, X. Ren, and H.C. Ott, *Perfusion decellularization of whole organs*. *Nat Protoc*, 2014. 9(6): p. 1451-68.
20. Leuning, D.G., F.M.R. Witjas, M. Maanaoui, A.M.A. de Graaf, E. Lievers, T. Geuens, C.M. Avramut, L.E. Wiersma, C.W. van den Berg, W. Sol, H. de Boer, G. Wang, V.L.S. LaPointe, J. van der Vlag, C. van Kooten, B.M. van den Berg, M.H. Little, M.A. Engelse, and T.J. Rabelink, *Vascular bioengineering of scaffolds derived from human discarded transplant kidneys using human pluripotent stem cell-derived endothelium*. *Am J Transplant*, 2018.
21. Hardy, R.J., *Molecular defects in the dysmyelinating mutant quaking*. *J Neurosci Res*, 1998. 51(4): p. 417-22.
22. Zearfoss, N.R., B.M. Farley, and S.P. Ryder, *Post-transcriptional regulation of myelin formation*. *Biochim Biophys Acta*, 2008. 1779(8): p. 486-94.

23. Luque, A., M. Gomez, W. Puzon, Y. Takada, F. Sanchez-Madrid, and C. Cabanas, *Activated conformations of very late activation integrins detected by a group of antibodies (HUTS) specific for a novel regulatory region (355-425) of the common beta 1 chain.* *J Biol Chem*, 1996. 271(19): p. 11067-75.
24. Tsuchida, J., S. Ueki, Y. Saito, and J. Takagi, *Classification of 'activation' antibodies against integrin beta1 chain.* *FEBS Lett*, 1997. 416(2): p. 212-6.
25. Somanath, P.R., E.S. Kandel, N. Hay, and T.V. Byzova, *Akt1 signaling regulates integrin activation, matrix recognition, and fibronectin assembly.* *J Biol Chem*, 2007. 282(31): p. 22964-76.
26. Virtakoivu, R., T. Pellinen, J.K. Rantala, M. Perala, and J. Ivaska, *Distinct roles of AKT isoforms in regulating beta1-integrin activity, migration, and invasion in prostate cancer.* *Mol Biol Cell*, 2012. 23(17): p. 3357-69.
27. Giaever, I. and C.R. Keese, *Use of Electric Fields to Monitor the Dynamical Aspect of Cell Behavior in Tissue Culture.* *IEEE Transactions on Biomedical Engineering*, 1986. BME-33(2): p. 242-247.
28. Junaid, A., A. Mashaghi, T. Hankemeier, and P. Vulto, *An end-user perspective on Organ-on-a-Chip: Assays and usability aspects.* *Current Opinion in Biomedical Engineering*, 2017. 1: p. 15-22.
29. Chistiakov, D.A., A.N. Orekhov, and Y.V. Bobryshev, *Effects of shear stress on endothelial cells: go with the flow.* *Acta Physiol (Oxf)*, 2017. 219(2): p. 382-408.
30. Erusalimsky, J.D., *Vascular endothelial senescence: from mechanisms to pathophysiology.* *J Appl Physiol (1985)*, 2009. 106(1): p. 326-32.
31. Harley, C.B., A.B. Futcher, and C.W. Greider, *Telomeres shorten during ageing of human fibroblasts.* *Nature*, 1990. 345(6274): p. 458-60.
32. Kaneko, T., S. Tahara, T. Taguchi, and H. Kondo, *Accumulation of oxidative DNA damage, 8-oxo-2'-deoxyguanosine, and change of repair systems during in vitro cellular aging of cultured human skin fibroblasts.* *Mutat Res*, 2001. 487(1-2): p. 19-30.
33. Chen, Q. and B.N. Ames, *Senescence-like growth arrest induced by hydrogen peroxide in human diploid fibroblast F65 cells.* *Proc Natl Acad Sci U S A*, 1994. 91(10): p. 4130-4.

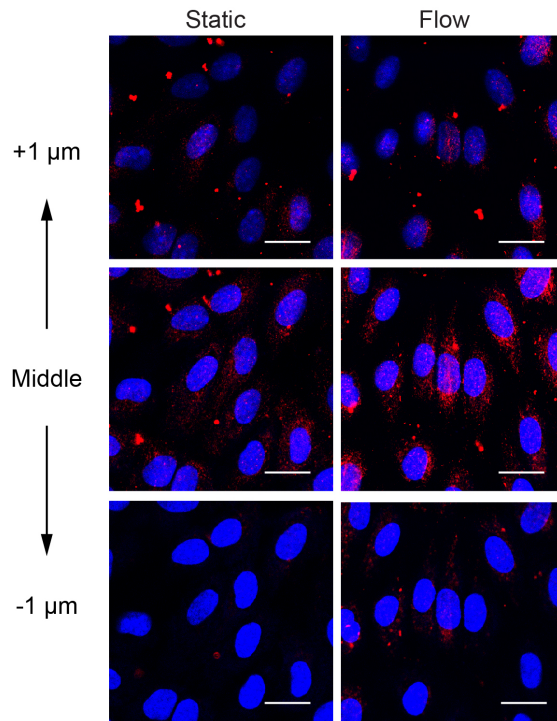
34. Li, L., Y. Hu, I. Ylivinkka, H. Li, P. Chen, J. Keski-Oja, and M. Hyytiainen, *NETRIN-4 protects glioblastoma cells FROM temozolomide induced senescence. PLoS One, 2013. 8(11): p. e80363.*
35. Lange, J., Y. Yafai, A. Noack, X.M. Yang, A.B. Munk, S. Krohn, I. Iandiev, P. Wiedemann, A. Reichenbach, and W. Eichler, *The axon guidance molecule Netrin-4 is expressed by Muller cells and contributes to angiogenesis in the retina. Glia, 2012. 60(10): p. 1567-78.*
36. Cheng, H.W., Y.F. Chen, J.M. Wong, C.W. Weng, H.Y. Chen, S.L. Yu, H.W. Chen, A. Yuan, and J.J. Chen, *Cancer cells increase endothelial cell tube formation and survival by activating the PI3K/Akt signalling pathway. J Exp Clin Cancer Res, 2017. 36(1): p. 27.*
37. Geiger, B. and A. Bershadsky, *Exploring the neighborhood: adhesion-coupled cell mechanosensors. Cell, 2002. 110(2): p. 139-42.*
38. Juliano, R.L., *Signal transduction by cell adhesion receptors and the cytoskeleton: functions of integrins, cadherins, selectins, and immunoglobulin-superfamily members. Annu Rev Pharmacol Toxicol, 2002. 42: p. 283-323.*
39. Yamamoto, H., M. Ehling, K. Kato, K. Kanai, M. van Lessen, M. Frye, D. Zeuschner, M. Nakayama, D. Vestweber, and R.H. Adams, *Integrin beta1 controls VE-cadherin localization and blood vessel stability. Nat Commun, 2015. 6: p. 6429.*
40. Larrieu-Lahargue, F., A.L. Welm, K.R. Thomas, and D.Y. Li, *Netrin-4 activates endothelial integrin alpha6beta1. Circ Res, 2011. 109(7): p. 770-4.*

Gene	Forward Sequence	Reverse Sequence
GAPDH	CCTGCACCACCAACTGCTTA	GGCCATCCACAGTCTTCTGAG
NTN1	GGGTGCCCTTCCAGTTCTAC	GCGAGTTGTCTGAAGTCGTG
NTN3	GCCGTTCGTCCCTTACTCCTA	TGAGGCATGTCCATTGCACTT
NTN4	GTACTTTGCGACTAACTGCTCC	TCCAGTGCATGGAAAAGGACT
NTN5	GGACCCATGCTACGATCCAC	AAGCGCAAGCTGACAGATGT
NTNG1	AAGTTTGGGATTACATGGCCTG	CGGAGGATCGAGTTTCACTTTC
NTNG2	GCGCCTGAAGGACTACGTC	CGTTGCTGCATAGGTAGGGAT
panQKI	CTGATGCTGTGGGACCTATTG	GTTGTTTGGCTGTAAGTCCTCT
ICAM-1	GGCCGGCCAGCTTATACAC	TAGACACTTGAGCTCGGGCA
VCAM-1	TCAGATTGGAGACTCAGTCATGT	ACTCCTCACCTTCCCGCTC
CDKN1A	ACTCTCAGGGTCGAAAACGG	CTTCCTGTGGGCGGATTAGG
CDKN1B	TCTGAGGACACGCATTTGGT	AAGAATCGTCGGTTGCAGGT
CDKN2A	GGAGGCCGATCCAGGTCAT	ACGGGTCGGGTGAGAGTG

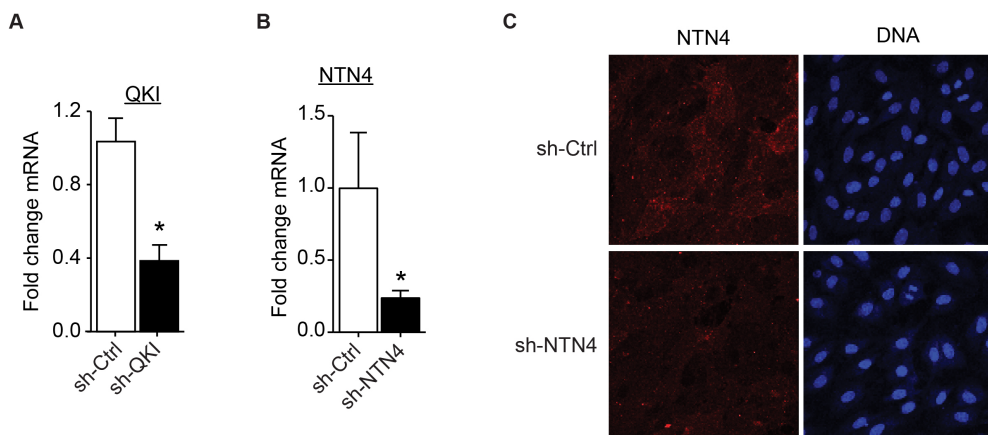
Supplemental table 1. List of primers

Antibody	Company	Catalogue number
Rabbit anti-human Akt	Cell Signaling	4691
Rabbit anti-human P-Akt	Cell Signaling	4060
Mouse anti-human CD31	BD Biosciences	555446
Mouse anti-human CDH5	BD Biosciences	555661
Goat anti-human CDKN1A	Santa Cruz Biotechnology	sc-397
Rabbit anti-human GAPDH	Cell Signaling	5174
Rabbit anti-goat HRP	Dako	P0160
Donkey anti-goat alexa-488	Invitrogen	A-11055
Donkey anti-goat alexa-568	Invitrogen	A-11057
Donkey anti-goat alexa-647	Invitrogen	A-21447
Rabbit anti-human ICAM1	Cell signaling	4915
Mouse anti-activated integrin β 1	Merck-Millipore	MAB2079Z
Mouse anti-integrin β 1	Santa Cruz Biotechnology	sc-53711
Rabbit anti-human laminin	Sigma Aldrich	L9393
Goat anti-mouse alexa-488	Invitrogen	A-11001
Goat anti-human NTN4	R&D Systems	AF1254
Mouse anti-panQKI	NeuroMab	clone N147/6
Goat anti-rabbit HRP	Dako	P0448
Donkey anti-rabbit alexa-568	Invitrogen	A-11011
Rabbit anti-human VCAM1	Abcam	ab134047

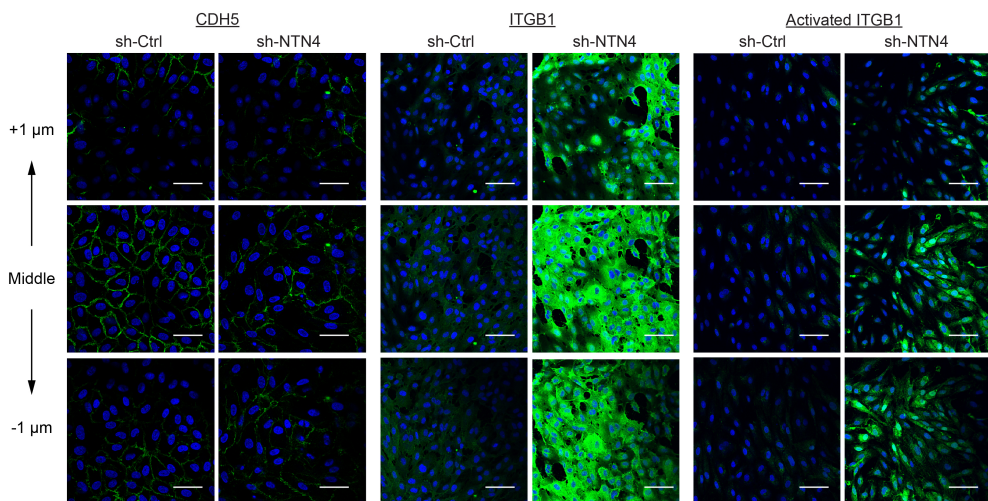
Supplemental table 2. List of antibodies used



Supplementary Figure 1. Immunofluorescent images at different z plane of staining of NTN4 (red) and DNA (blue) in HUVECs cultured under static conditions or laminar flow (10 dynes/cm²). Scale bar = 20 μm.



Supplementary Figure 2. (A) qPCR analysis of QKI mRNA isolated from HUVECs transduced with anti-Qki shRNA (sh-QKI) or control shRNA (sh-Ctrl). Results are presented relative to sh-Ctrl. Mean \pm SEM of $n = 5$. * $p < 0.05$. (B) NTN4 mRNA expression in sh-RNA treated endothelial cells (sh-Ctrl) or endothelial cells treated with sh-RNA against NTN4 (sh-NTN4). Results are presented relative to scrambled. Mean \pm SEM of $n = 3$; * $p < 0.05$. (C) Immunofluorescence staining of NTN4 (red) and DNA (blue) in HUVECs transduced with anti-NTN4 shRNA (sh-NTN4) or scrambled shRNA (sh-Ctrl).



Supplementary Figure 3. Immunofluorescent images at different z plane of staining of CDH5, integrin β 1 or activated integrin β 1 (green) and DNA (blue) in HUVECs transduced with anti-NTN4 shRNA (sh-NTN4) or scrambled shRNA (sh-Ctrl). Representative images of $n = 2-3$. Scale bar = 50 μ m.